ISSN (Print) 1226-1750
ISSN (Online) 2233-6656
Journal of Magnetics 28(1), 56-63 (2023) https://doi.org/10.4283/JMAG.2023.28.1.056

Feasibility Study of Block-Matching and 3D Filtering Algorithm in Low-Dose CT Image with Tin Filter

Mingyu Song[1], Minsu Kim[1], Junsoo Lim[1], Donghwan Chun[1], Minji Park[2], Jina Shim[3]*, and Youngjin Lee[1]*

[1]*Department of Radiological Science, Gachon University, 191, Hambakmoero, Yeonsu-gu, Incheon, Republic of Korea*
[2]*Department of Health Science, General Graduate School of Gachon University, 191, Hambakmoero, Yeonsu-gu, Incheon, Republic of Korea*
[3]*Department of Radiology, Severance Hospital, 50-1, Yonsei-ro, Seodaemun-gu, Seoul, Republic of Korea*

(Received 3 March 2023, Received in final form 21 March 2023, Accepted 27 March 2023)

The purpose of this study was to confirm the utility of block-matching and 3D filtering (BM3D) algorithm in computed tomography (CT) images using a tin filter with a high pitch. We acquired phantom images and measured the coefficient of variation (COV) and contrast-to-noise ratio (CNR) for quantitative evaluation. The optimized results were obtained when the sigma value of the BM3D algorithm was nine. In addition, when the sigma value of the optimized BM3D algorithm was applied, superior results were obtained compared with conventional filtering methods. In particular, we confirmed that the COV and CNR of the images obtained using the BM3D algorithm improved 6.52 and 5.49 times, respectively. In conclusion, the utility of the optimized BM3D algorithm has been demonstrated in low-dose CT images using a tin filter.

Keywords : radio-magnetic imaging, low-dose CT, Tin filter, radio-magnetic image processing, block-matching and 3D filtering (BM3D), optimization of denoising algorithm

1. Introduction

According to the NCRP 184 report released in 2019, the number of computed tomography (CT) scans increased by approximately 25 %, from 67 to 84 million per year from 2006 to 2016 [1]. As the number of examinations increased, the research on reduction of exposure dose also increased steadily; however, the exposure dose did not fundamentally decrease from 1.46 to 1.37 mSv per person in 2006 and 2016, respectively. Therefore, methods for reducing the exposure dose are continuously being studied.

One method uses a high pitch to reduce the exposure dose. The pitch is the value obtained by dividing the distance traveled by the patient table during one rotation of the radiograph tube by the slice thickness. When the pitch increases, the exposure dose can be reduced by reducing the time required for the examination.

*Corresponding author: Tel: +82-2-2228-7396,
Fax: +82-2-2229-7396, e-mail: eoeornfl@yonsei.ac.kr
Tel: +82-32-820-4362, Fax: +82-32-820-4449,
e-mail: yj20@gachon.ac.kr

Another method for reducing the exposure dose involves the use of additional filters. Additional filters are used to reduce the exposure dose by eliminating the low-energy radiographs reaching the patient. Aluminum materials have been widely used as conventional additional filters, but there are many limitations in using them in the field of X-ray imaging. Among various additional filters, a method using tin filters has been proposed to improve X-ray system performance [2-5]. Using a tin filter as an additional filter for low-dose CT scans can improve the spatial resolution of the image by absorbing the low-energy spectrum from the tube-voltage spectrum and examining it using a suitable spectrum for low-dose scanning. In addition, a tin filter has little effect on the spatial frequency and thus does not affect the image texture; the half-value layer increases by 64-82 %, and the average weight energy increases by 29-37 % [6].

However, the use of a high pitch or an additional filter causes noise in the image owing to a decrease in the number of photons that reach the detector directly [7]. Therefore, various image filtering algorithms have been proposed to reduce this noise [8-10]. The median and Wiener filters are representative algorithms. The median

filter divides an image into several pixels and uses an intermediate value instead of the neighboring pixels. The median filter has the disadvantage of acting uniformly over the entire area with and without noise, deteriorating the entire edge and visually important areas. The Wiener filter minimizes the mean square error between the original and reconstructed images based on the assumption that additional noise is generated by a static random process, regardless of the pixel position, while providing excellent high-frequency characteristics, effectively removing noise in a flat region, and preserving edge components. However, since denoising is primarily performed on flat areas in X-ray image, noise reduction in areas with many edges will be degraded [11, 12].

To compensate for these disadvantages, a block-matching and 3D filtering algorithm (BM3D) was developed. The BM3D algorithm performs two filtering steps using different filtering in three-dimensional regions, each step involving hard thresholding and Wiener filtering [13]. The BM3D algorithm uses a noise removal method based on block-matching and is based on experimental observations that adjacent patches or blocks of images have similar features. It has proven to perform well in removing various types of noise [14].

In this study, after acquiring images to which the BM3D algorithm was applied in tin-filter-based low-dose high-pitch CT images, we determined the effectiveness of the BM3D algorithm by obtaining the contrast-to-noise ratio (CNR) and coefficient of variation (COV) for quantitative evaluation using MATLAB.

2. Materials and Methods

2.1. Phantom and CT Device

Table 1. The parameters for acquisition of normal and low-dose CT images. The kVp and mA of the two groups were set identically, and the rotation time and pitch were set differently.

CT parameter \ Group	Group 1	Group 2
kV	100	100
mA	Care Dose 4D	Care Dose 4D
Rotation time (s)	0.5	0.25
Detector collimation (mm)	192*0.6	192*0.6
Pitch	0.8	2.5
Filter	Sn	Sn

The phantom used in this study was an AAPM CT Performance Phantom (CIRS, Norfolk, USA), and the CT device used for the examination was a SOMATOM Force (Siemens Healthcare, Erlangen, Germany).

2.2. Experimental design

In this study, the image using a tin filter was set as the control group, and the image using a tin filter and high pitch was set as the comparison group. Group 1 (control group) had a pitch of 0.8 and a tin filter was used. Group 2 (comparison group) had a pitch of 2.5 and a tin filter was used similar to the control group.

The conditions used to scan the phantoms are listed in Table 1. For Group 1, a tube voltage of 10 kV and current of Care Dose 4D, rotation time of 0.5 s, detector collimation of 192×0.6 mm, pitch of 0.8, and tin filter were used. For Group 2, a tube voltage of 100 kV and current of Care Dose 4D, rotation time of 0.25 s, detector collimation of 192×0.6 mm, pitch of 2.5, and tin filter were used.

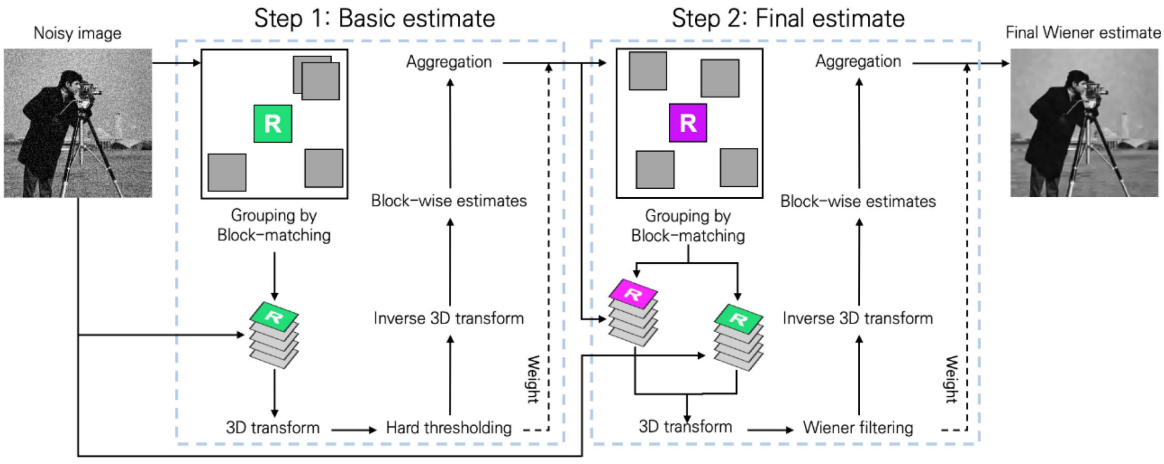

Fig. 1. (Color online) Scheme of the BM3D algorithm modeling in this study. The BM3D algorithm includes the process of going through the final estimation process after the basic estimation from the noisy image.
BM3D, block-matching and 3D filtering

2.3. BM3D algorithm modeling

The BM3D algorithm used in this study performs two filtering stages using different filtering methods in a three-dimensional domain [15]. Hard thresholding and Wiener filtering were performed in each step (Fig. 1).

2.3.1. The first denoising step (hard thresholding)

Similar images were collected to form a three-dimensional group. In one loop, a window of size $n^{ht} \times n^{ht}$ was specified, and the reference patch of size $k^{ht} \times k^{ht}$ at the center of the window was designated as *P*. In the window, patch *Q* similar to patch *P* were selected and stored in a three-dimensional arrangement. Grouping was performed after measuring the dissimilarity using the L_2-norm. The arrangement $\mathcal{P}(P)$ of similar patches was expressed as follows:

$$\mathcal{P}(P) = \left\{ d(P,Q) = \frac{\|\gamma'(P) - \gamma'(Q)\|_2^2}{(k^{ht})^2} \leq \tau^{ht} \right\} \quad (1)$$

where τ^{ht} is the maximum distance between patches where two patches are considered similar; γ' is a hard thresholding operator using a 2D threshold; $d(P, Q)$ is a 2D distance between normalized patches.

Once the arrangement $\mathcal{P}(P)$ of similar patches was built, a 3D group $\mathbb{P}(P)$ was created by stacking $\mathcal{P}(P)$. A unitary 3D transform was applied, followed by noise attenuation by hard thresholding of the transform coefficients. An inverse linear transform was then applied to estimate each patch. The 3D group $\mathbb{P}(P)$ had the following characteristics:

$$\mathbb{P}(P)^{ht} = \tau_{3D}^{ht^{-1}} \left\{ \gamma \left[\tau_{3D}^{ht} \left(\mathbb{P}(P) \right) \right] \right\} \quad (2)$$

where the hard threshold operator γ with 3D threshold was as follows:

$$\gamma(x) = \begin{cases} 0 & if\ |x| \leq \gamma_{3D}^{ht} \sigma \\ x & otherwise \end{cases} \quad (3)$$

The group created in the grouping process was subjected to 2D DCT in each patch and 1D DCT in the three-dimension direction for 3D transformation.

When the collaborative filtering was completed, the estimated value for each patch was obtained, and the estimates for every pixel were then obtained. The estimates were as follows:

$$\forall Q \in \mathcal{P}(P),\ \forall_x \in Q, \begin{cases} \nu(x) = \nu(x) + \omega_P^{ht} u_{Q,P}^{ht}(x) \\ \delta(x) = \delta(x) + \omega_P^{ht} \end{cases} \quad (4)$$

where ν (resp. δ) is the numerator of the basic estimation of the image obtained at the end of collaborative filtering, $u_{Q,P}^{ht}(x)$ is the estimation of pixel *x* belonging to the patch *Q* obtained during collaborative filtering of the reference patch *P*, $\omega_{\mathrm{P}}^{\mathrm{ht}} = \begin{cases} (\mathrm{N}_{\mathrm{P}}^{\mathrm{ht}})^{-1} & if\ N_P^{ht} \geq 1 \\ 1 & otherwise \end{cases}$, and N_P^{ht} is the number of coefficients remaining in 3D block after hard thresholding.

The basic estimate obtained after the first denoising step can be expressed as follows:

$$u^{basic}(x) = \frac{\sum_P \omega_P^{ht} \sum_{Q \in \mathcal{P}(P)} \chi_Q(x) u_{Q,P}^{ht}(x)}{\sum_P \omega_P^{ht} \sum_{Q \in \mathcal{P}(P)} \chi_Q(x)} \quad (5)$$

2.3.2. The final denoising step (Wiener filtering)

In this step, the basic estimate u^{basic} obtained in the first denoising step was used. The final denoising step performed Wiener filtering to restore more details and improve the denoising performance. Patch matching was performed only for basic estimates. When $\mathcal{P}^{basic}(P) = \{Q : d(P,Q) \leq \tau^{wie}\}$, a set of similar patches was obtained, two 3D groups were formed. $\mathbb{P}^{basic}(P)$ was formed by stacking patches in the basic estimation u^{basic} and $\mathbb{P}(P)$ by stacking patches of the same order as in the original noisy image *u*. Collaborative filtering was performed when two 3D groups were obtained. To achieve this, the empirical Wiener coefficients were defined as follows:

$$\omega_P(\xi) = \frac{\left| \tau_{3D}^{wie}(\mathbb{P}^{basic}(P))(\xi) \right|^2}{\left| \tau_{3D}^{wie}(\mathbb{P}^{basic}(P))(\xi) \right|^2 + \sigma^2} \quad (6)$$

The collaborative filtering of $\mathbb{P}(P)$ implemented the 3D transformation of the noisy image $\tau^{wie}(\mathbb{P}(P))$ by elementwise multiplication using Wiener coefficients ω_P. The 3D group estimated using this process was expressed as follows:

$$\mathbb{P}^{wie}(P) = \tau_{3D}^{wie^{-1}} \left[\omega_P \cdot \tau_{3D}^{wie} \left(\mathbb{P}(P) \right) \right] \quad (7)$$

After collaborative filtering, the estimates for each pixel were stored in a buffer as follows:

$$\forall Q \in \mathcal{P}(P),\ \forall_x \in Q, \begin{cases} \nu(x) = \nu(x) + \omega_P^{wie} u_{Q,P}^{wie}(x) \\ \delta(x) = \delta(x) + \omega_P^{wie} \end{cases} \quad (8)$$

where ν (resp. δ) is the numerator of the final estimation of the image obtained at the end of collaborative filtering, $u_{Q,P}^{wie}(x)$ is the estimate of pixel *x* of patch *Q* obtained during collaborative filtering of reference patch *P*, and $\omega_P^{wie} = \|\omega_P\|_2^{-2}$..

The final estimation obtained in the final denoising step was as follows:

$$u^{final}(x) = \frac{\sum_P \omega_P^{wie} \sum_{Q \in \mathcal{P}(P)} \chi_Q(x) u_{Q,P}^{wie}(x)}{\sum_P \omega_P^{wie} \sum_{Q \in \mathcal{P}(P)} \chi_Q(x)} \quad (9)$$

$$\left(\chi_Q(x) = \begin{cases} 1 & if \quad x \in Q \\ 0 & otherwise \end{cases} \right)$$

2.4. Quantitative evaluation of image quality

The sigma value, which is the Wiener filtering adjustment parameter in the BM3D algorithm, was set from 1 to 15 and quantitatively evaluated to derive the optimal sigma value. Then, the image to which the optimized BM3D algorithm was applied was quantitatively compared with the original, median-filtered, and Wiener-filtered images. The parameters used for the quantitative evaluation were CNR and COV.

CNR was obtained by dividing the signal average by the standard deviation, and the equation is as follows:

$$CNR = \frac{\left|ROI\ SI_{Avg} - BKG\ SI_{Avg}\right|}{\sqrt{ROI\ SD^2 + BKG\ SD^2}} \tag{10}$$

where $ROI\ SI_{Avg}$ and $BKG\ SI_{Avg}$ denote the average values of the signals in the region of interests (ROI) and background (BKG), respectively; and *ROI SD* and *BKG SD* denote the standard deviations in the ROI and BKG,

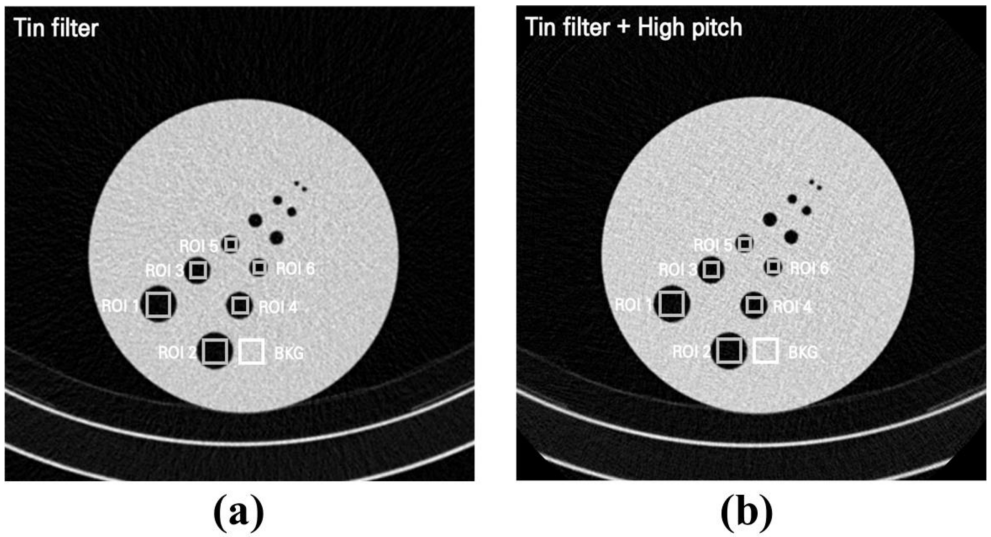

Fig. 2. AAPM CT performance phantom images using (a) tin filter and (b) tin filter + high pitch with region of interests (ROIs) for quantitative evaluation. The ROI was set in the same area for each image.

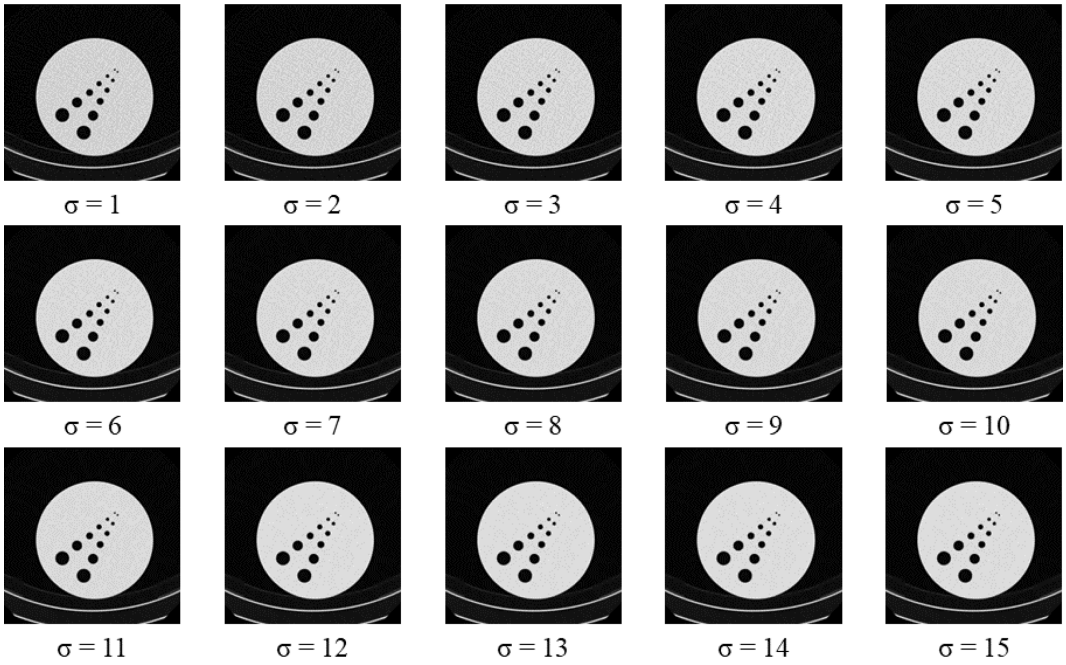

Fig. 3. Denoised images acquired by changing the sigma value from 1 to 15. As the sigma value is increased, it can be visually confirmed that the noise parts of the obtained CT image are reduced.

respectively.

The COV was obtained by dividing the standard deviation of the ROI by the signal average, and the equation is as follows:

$$COV = \frac{ROI\ SD}{ROI\ SI_{Avg}} \quad (11)$$

Fig. 2 shows a diagram of the ROI and BKG setups. Six ROIs were set and the mean values of the CNR and COV were obtained to compare the algorithms.

3. Results and Discussion

Fig. 3 shows images in which the BM3D algorithm was applied with different sigma values from 1 to 15 to the image using tin filters with high pitch. The CNR and COV were measured to quantitatively evaluate the noise intensity and derive the optimal sigma value. ROIs of the same size and position as the ROI set shown in Fig. 2 were applied to each image. Tables 2 and 3 show the calculated CNR and COV results, respectively. Fig. 4 shows a graph of the average values of CNR and COV. For CNR, the values started to converge at a sigma value of 8-9, whereas for COV, the values started to converge at a sigma value of 5-6. Considering the contrast aspect, the optimal sigma value was determined to be 9.

To examine the effectiveness of the BM3D algorithm, we first acquired images in which the median and Wiener filters were applied to the image using a tin filter with high pitch (Fig. 5). Table 4 shows the mean CNR values calculated in six ROIs of the images using the tin filter and the tin filter with high pitch, and median-filtered, Wiener-filtered, and BM3D-filtered images. The calculated CNRs for the images using the tin filter and tin filter with high pitch, and median-filtered, Wiener-filtered, and BM3D-filtered images were 17.6349±1.6416, 15.8605± 0.1849, 23.7375±0.6095, 25.3549±0.6593, and 87.1633± 8.0696, respectively. Table 5 shows the mean values of the COV calculated in six ROIs of the images using the tin filter and tin filter with high pitch, and median-filtered, Wiener-filtered, and BM3D-filtered images. The calculated COVs for the images using the tin filter and tin filter with

Table 2. Results of CNR as a function of sigma value. The CNR result values of 6 ROIs were derived for each sigma value, and the values were expressed as average values and standard deviations.

	σ=1	σ=2	σ=3	σ=4	σ=5
ROI1	16.1243	18.7910	23.2925	29.7191	38.4153
ROI2	16.0803	18.5239	23.2495	30.2960	39.3738
ROI3	16.3048	18.9582	23.6498	30.7997	40.7779
ROI4	16.4397	19.8692	24.8468	31.5076	41.0002
ROI5	16.0623	18.4435	23.0696	30.3948	40.4053
ROI6	16.6492	19.4380	24.6958	31.2093	40.4520
Mean	16.2768±0.2340	19.0040±0.5530	23.8007±0.7765	30.6544±0.6523	40.0708±0.9846
	σ=6	σ=7	σ=8	σ=9	σ=10
ROI1	52.6706	67.1176	73.0045	76.7586	78.9025
ROI2	53.8659	69.7619	75.0676	78.3212	79.9202
ROI3	59.2507	80.5511	89.4320	91.5111	89.2745
ROI4	59.0281	82.6252	94.2605	97.0656	99.9054
ROI5	58.3465	80.1160	89.3003	91.8653	91.1798
ROI6	56.1981	73.2273	81.9892	87.4580	89.9160
Mean	56.5600±2.7943	75.5665±6.4175	83.8424±8.5728	87.1633±8.0696	88.1831±7.8101
	σ=11	σ=12	σ=13	σ=14	σ=15
ROI1	81.2861	84.1241	85.6459	89.1145	90.6479
ROI2	81.7088	81.3994	83.3727	81.5036	81.8386
ROI3	87.7073	90.3277	91.8375	91.5483	91.5131
ROI4	101.6459	105.8142	109.2210	111.1545	111.0998
ROI5	88.1670	94.1389	91.3461	94.6132	91.1040
ROI6	88.7171	93.0768	94.0858	89.6750	88.3862
Mean	88.2054±7.3653	91.4802±8.6272	92.5848±9.1008	92.9349±9.9256	92.4316±9.8272

CNR, contrast-to-noise ratio; ROI, region of interest

Table 3. Results of COV as a function of sigma value. The COV result values of 6 ROIs were derived for each sigma value, and the values were expressed as average values and standard deviations.

COV	σ=1	σ=2	σ=3	σ=4	σ=5
ROI1	0.6746	0.5072	0.3452	0.2502	0.2135
ROI2	0.6421	0.5061	0.3286	0.1775	0.1468
ROI3	0.6944	0.5334	0.3424	0.1763	0.0945
ROI4	0.6574	0.3900	0.1679	0.0686	0.0653
ROI5	0.8318	0.6982	0.4677	0.2357	0.1226
ROI6	0.9227	0.6540	0.3097	0.2234	0.1951
Mean	0.7372±0.1136	0.5482±0.1117	0.3269±0.0959	0.1886±0.0662	0.1396±0.0573
	σ=6	σ=7	σ=8	σ=9	σ=10
ROI1	0.2024	0.1986	0.1987	0.1855	0.1812
ROI2	0.1529	0.1534	0.1634	0.1523	0.1511
ROI3	0.0444	0.0732	0.0906	0.0931	0.1260
ROI4	0.0539	0.0313	0.0313	0.0313	0.0222
ROI5	0.0850	0.0797	0.0910	0.0901	0.1114
ROI6	0.2069	0.2151	0.2074	0.1779	0.1746
Mean	0.1243±0.0730	0.1252±0.0746	0.1304±0.0702	0.1217±0.0603	0.1278±0.0583
	σ=11	σ=12	σ=13	σ=14	σ=15
ROI1	0.1733	0.1703	0.1708	0.1599	0.1542
ROI2	0.1481	0.1623	0.1638	0.1795	0.1807
ROI3	0.1473	0.1473	0.1513	0.1610	0.1610
ROI4	0.0222	0.0222	0.0222	0.0222	0.0222
ROI5	0.1421	0.1200	0.1527	0.1392	0.1595
ROI6	0.1952	0.1847	0.1919	0.2344	0.2519
Mean	0.1380±0.0602	0.1345±0.0593	0.1421±0.0606	0.1494±0.0702	0.1549±0.0745

COV, coefficient of variation; ROI, region of interest

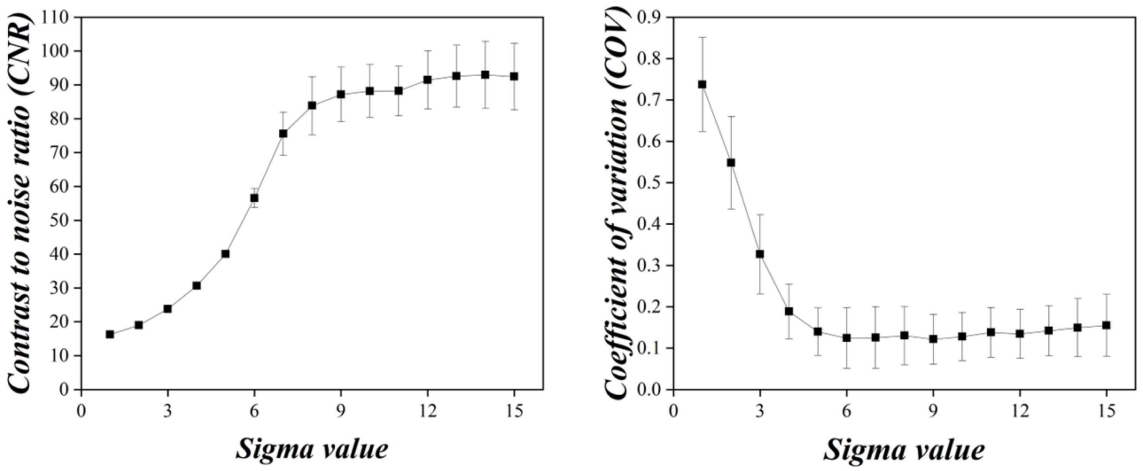

Fig. 4. (a) CNR and (b) COV value graph of six ROIs according to sigma value. Both the CNR and COV result graphs showed a tendency for the values to converge from a certain range as the sigma value changed.
CNR, contrast-to-noise ratio; COV, coefficient of variation; ROI, region of interest

high pitch, and median-filtered, Wiener-filtered and BM3D-filtered images were 0.8041±0.0682, 0.7942± 0.1232, 0.5559±0.0974, 0.4808±0.0842 and 0.1217± 0.0603, respectively.

Fig. 6 shows a comparison of the CNR and COV for the images using a tin filter, tin filter with a high pitch,

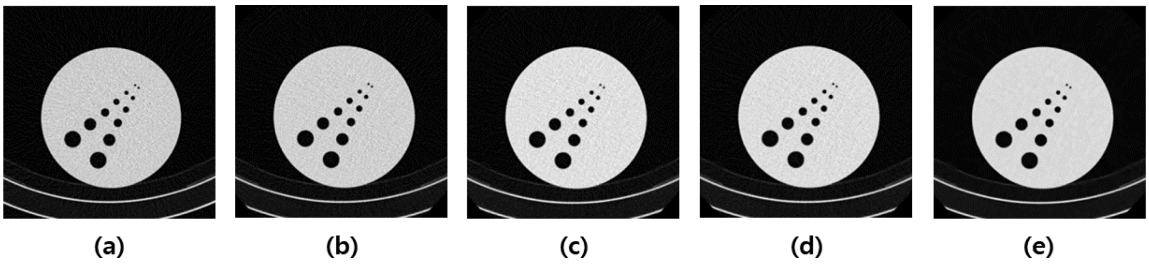

Fig. 5. Resulting images using various denoising algorithm: (a) tin filter, (b) tin filter + high pitch, (c) median filtering applied to (b), (d) Wiener filtering applied to (b), and (e) proposed BM3D algorithm (sigma value 9) applied to (b). When the optimized BM3D algorithm was applied, it was confirmed that the noise of the image was visually improved.
BM3D, block-matching and 3D filtering

Table 4. CNR value for each acquired image. The proposed BM3D algorithm showed the best CNR results.

	Tin filter	Tin filter + High pitch	Median filter	Wiener filter	BM3D
CNR	17.6349±1.6416	15.8605±0.1849	23.7375±0.6095	25.3549±0.6593	87.1633±8.0696

CNR, contrast-to-noise ratio; BM3D, block-matching and 3D filtering

Table 5. COV value for each acquired image. The proposed BM3D algorithm showed the best COV results.

	Tin filter	Tin filter + High pitch	Median filter	Wiener filter	BM3D
COV	0.8041±0.0682	0.7942±0.1232	0.5559±0.0974	0.4808±0.0842	0.1217±0.0603

COV, coefficient of variation; BM3D, block-matching and 3D filtering

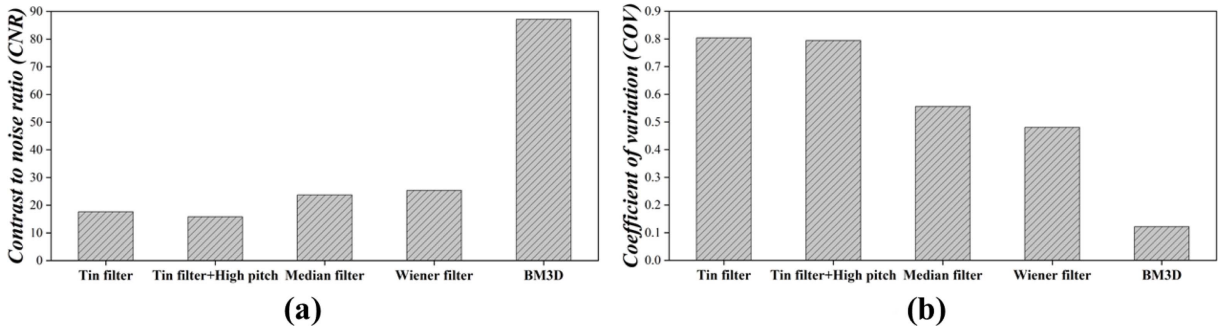

Fig. 6. Graphs of (a) CNR and (b) COV values with respect to the denoising algorithm. The excellent CNR and COV results were shown when the proposed BM3D algorithm was applied to the acquired images.
CNR, contrast-to-noise ratio; COV, coefficient of variation

and tin filter with a high pitch applied with a median filter, Wiener filter, and BM3D algorithm. When the algorithm was applied, the CNR increased by about 1.49, 1.59, and 5.49 times compared to that with the original image and COV increased by about 1.42, 1.65, and 6.52 times compared to that with the original image. Moreover, when the BM3D algorithm was applied, the noise was reduced more effectively than that with median and Wiener filters. Based on the results, we expect that applying the optimized BM3D algorithm to low-dose CT images with a tin filter could reduce patients' exposure dose and improve image quality compared to conventional CT scan images.

CT images are indispensable for the early diagnosis of lesions in the diagnostic medical field, and the number of examinations has been gradually increasing [16, 17]. Particularly, because children are more sensitive to radiation, a low-dose-based scanning method is essential for performing CT scans in them [18]. According to the study results of Brenner *et al*., the risk of cancer mortality by undergoing abdominal and head CT examinations performed at 1 year of age was significant and at 0.18 and 0.07 %,

respectively [19]. Compared to adults, it is considered a more meaningful value for children who are very sensitive to radiation, and we expect the BM3D algorithm proposed in this study to be useful in this regard.

A limitation of this study is that the evaluation was conducted only with images using phantoms. We expect that a more accurate image evaluation will be possible if the BM3D algorithm is applied to low-dose CT images using a high pitch and tin filters through images obtained from patients in the future. In addition, among CT image reconstruction methods, we expect that the iterative-based method that can acquire high-quality image characteristics with a low dose compared to the filtered backprojection can further improve the efficiency of the BM3D algorithm [20].

4. Conclusion

In this study, we demonstrated that the application of the BM3D algorithm to low-dose CT images using a tin filter and high pitch was effective in improving the image quality using the AAPM CT performance phantom. In conclusion, applying the BM3D algorithm to a tin-filter-based low-dose CT image can reduce patients' exposure dose and improve the image quality compared to that through conventional CT images without a high pitch.

Acknowledgement

This study was supported by the National Research Foundation of Korea (NRF-2021R1F1A1061440).

References

[1] F. A. Mettler, M. Mahesh, M. Bhargavan-Chatfield, C. E. Chambers, J. G. Elee, D. P. Frush, D. L. Miller, H. D. Royal, M. T. Milano, D. C. Spelic, A. J. Ansari, W. E. Bolch, G. M. Guebert, R. H. Sherrier, J. M. Smith, and R. J. Vetter, Radiology **295**, 418 (2020).

[2] S. Kaufmann, A. Sauter, D. Spira, S. Gatidis, D. Ketelsen, M. Heuschmid, C. D. Claussen, and C. Thomas, Acad. Radiol. **20**, 596 (2013).

[3] H. Haubenreisser, M. Meyer, S. Sudarski, T. Allmendinger, S. O. Schoenberg, and T. Henzler, Eur. J. Radiol. **84**, 1608 (2015).

[4] M. M. Lell, M. M. Brand, A. Eller, T. Buder, E. Hofmann, M. Uder, and W. Wuest, Am. J. Neuroradiol. **36**, 1225 (2015).

[5] A. Mozaffary, T. A. Trrabzonlu, D. Kim, and V. Yaghmai, AJR **212**, 1 (2019).

[6] J. Greffier, F. Pereire, A. Hamard, T. Addala, J. P. Beregi, and J. Frandon, Diagn. Interv. Imaging **101**, 373 (2020).

[7] Y. Sagara, A. K. Hara, W. Pavlicek, A. C. Silva, R. G. Paden, and Q. Wu, AJR **195**, 713 (2010).

[8] W. A. Kalender, E. Klotz, and L. Kostaridou, IEEE Trans. Med. Imaging **7**, 218 (1988).

[9] M. C. Pan and A. H. Lettington, Proceedings. IEEE International Joint Symposia on Intelligence and Systems (Cat. No.98EX174), DOI: 10.1109/IJSIS.1998.685472 (1998).

[10] T. D. Pham, Pattern Recognition 34, 2403 (2001).

[11] L. Zhang and H. Yin, Eighth IEEE/ACIS International Conference on Computer and Information Science, DOI: 10.1109/ICIS.2009.51 (2009).

[12] P. Chan and J. S. Lim, IEEE Trans. Acoust. **ASSP-33**, 117 (1985).

[13] K. Dabov, A. Foi, V. Katkovnik, and K. Egiazarian, IEEE Trans. Image Process. **16**, 2080 (2007).

[14] L. L. Chen, S. P. Gou, Y. Yao, J. Bai, L. Jiao, and K. Sheng, IEEE Region 10 Conference (TENCON), DOI: 10.1109/TENCON.2016.7848089 (2017).

[15] M. Lebrun, Image Processing On Line 2, 175 (2012).

[16] J. Y. Jeon, S. W. Lee, Y. M. Jeong, and H. J. Baek, Eur. Radiol. **29**, 1248 (2019).

[17] S. J. Kim, S. J. Ahn, S. J. Choi, D. H. Park, H. S. Kim, and J. H. Kim, Am. J. Emerg. Med. **37**, 1331 (2019).

[18] G. Chodick, K. P. Kim, M. Shwarz, G. Horev, V. Shalev, and E. Ron, Pediatr. Endocrinol. Rev. **7**, 29 (2009).

[19] D. J. Brenner, C. D. Elliston, E. J. Hall, and W. E. Berdon, AJR 176, 289 (2001).

[20] J. H. Hwang, J. M. Kang, S. H. Park, S. Park, J. H. Kim, and S. T. Choi, PLOS ONE 16, doi.org/10.1371/journal.pone.0256564 (2021).